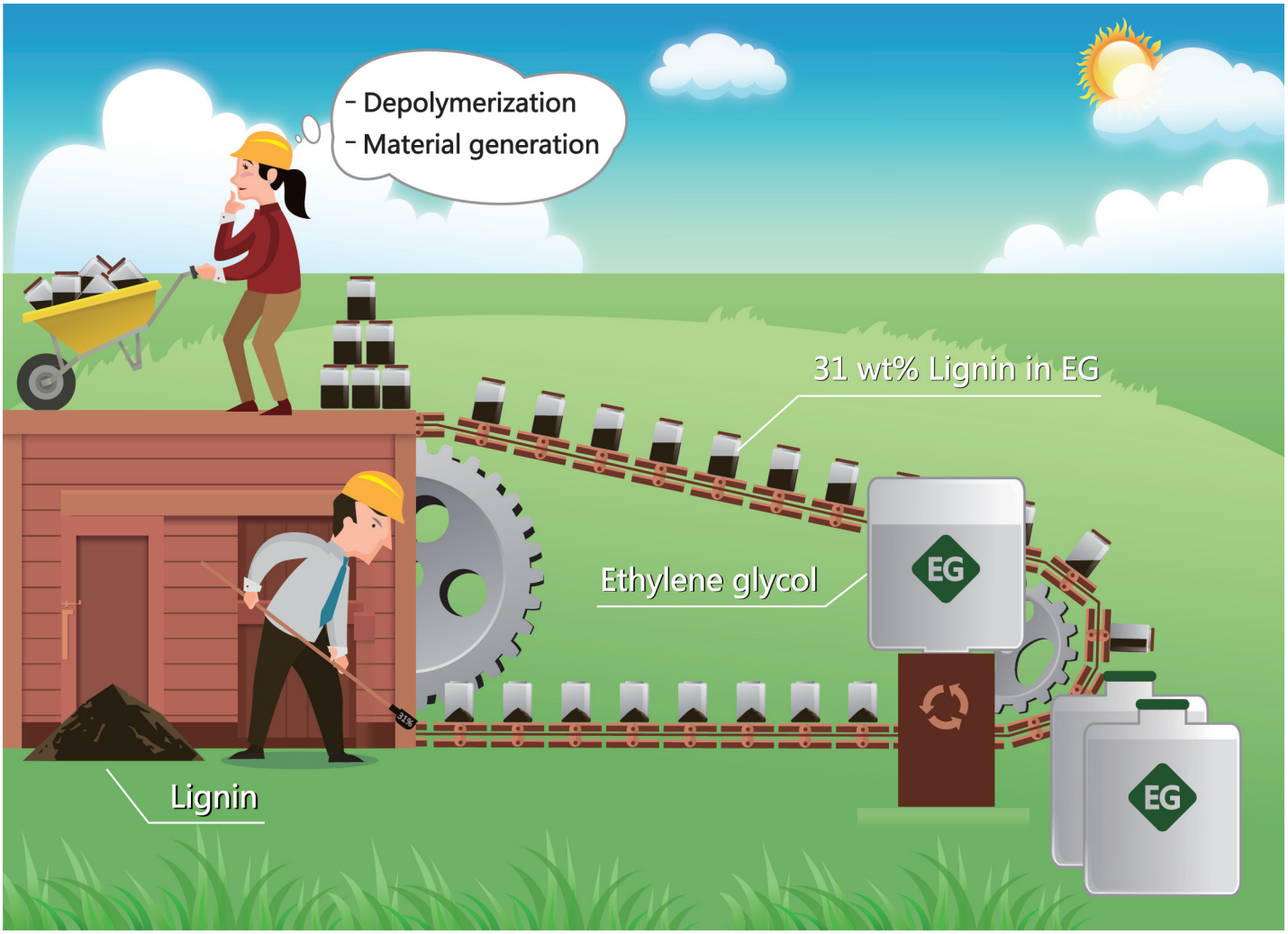

An article presented by Dr. Jian Sun *et al.* as joint research of the Joint BioEnergy Institute (JBEI); Lawrence Berkeley National Laboratory (LBNL); Sandia National Laboratories (SNL); Environmental Molecular Sciences Laboratory (EMSL); and Pacific Northwest National Laboratory (PNNL).

Rapid room temperature solubilization and depolymerization of polymeric lignin at high loadings

The relatively poor solubility of lignin in most solvents is one of the foremost challenges in lignin valorization to improve biorefinery economics. This study demonstrates rapid room temperature solubilization of polymeric lignin at high loading in ethylene glycol, which can be directly applied for utilization of lignin. This finding also provides mechanistic insights into H-bond interactions in lignin dissolution.

As featured in:

See Seema Singh *et al.*, *Green Chem.*, 2016, **18**, 6012.

ROYAL SOCIETY OF CHEMISTRY

www.rsc.org/greenchem

Registered charity number: 207890

Green Chemistry

PAPER

View Article Online
View Journal | View Issue

Cite this: *Green Chem.*, 2016, **18**, 6012

Rapid room temperature solubilization and depolymerization of polymeric lignin at high loadings†

Jian Sun,[a,b] Tanmoy Dutta,[a,b] Ramakrishnan Parthasarathi,[a,b] Kwang Ho Kim,[a,b] Nikola Tolic,[c] Rosalie K. Chu,[c] Nancy G. Isern,[c] John R. Cort,[c,d] Blake A. Simmons[a,e] and Seema Singh*[a,b]

Received 13th August 2016,
Accepted 3rd October 2016

DOI: 10.1039/c6gc02258h

www.rsc.org/greenchem

The relatively poor solubility of lignin in most pretreatment solvents remains one of the biggest challenges in lignin valorization to improve overall biorefinery economics. In this work, rapid room temperature solubilization of lignin at high solid loadings (>30 wt%) can be easily achieved in a single step using ethylene glycol (EG). The solubilized lignin can be rapidly and quantitatively recovered with the addition of ethanol. The computational and nuclear magnetic resonance (NMR) spectroscopic studies confirm that strong hydrogen bond interactions between EG and the free hydroxyl groups present in lignin contribute to the lignin dissolution. In addition, hydrogen peroxide mediated depolymerization of the dissolved lignin at a low temperature (80 °C) was tested and the effect of EG molecules on depolymerization of lignin was also theoretically studied. The findings of this work provide mechanistic insights of hydrogen bond interactions in high lignin solubilization and valorization.

Introduction

Lignin, the primary aromatic component of lignocellulosic biomass, is an abundant renewable resource.[1,2] However, it has been typically underused as a waste stream in most current bio-refinery processes and burned for generation of heat.[1,2] There has been significant work on the production of alternative fuels,[1] renewable chemicals,[3] value-added polymeric materials[4] and platform compounds[5] from lignin over the past few decades, and the role of effective utilization of lignin in improving the economics of the lignocellulosic biorefinery has been widely acknowledged.[3,6]

The complex, highly cross-linked structure of lignin is a major barrier that must be addressed in order to efficiently and affordably valorize this biopolymer.[1–4] Although a variety of catalytic, thermal, and biological approaches have been employed to break lignin down to its constituent monomers,[2,7,8] upgrading lignin and lignin-derived intermediates into useful chemicals or fuels, which is also known as liquefaction of lignin, is still at a relatively early stage and presents significant technical challenges.[9,10] From the technoeconomic standpoint, efficient solubilization of lignin as well as simple isolation of the solvent is highly desirable.[11–13] To this end, various new solvents have been explored and ionic liquids (ILs) are among the most effective lignin solvents known.[14] Although imidazolium, cholinium and pyrrolidinium based ILs have demonstrated high lignin solubility, they typically require a basic pH environment, high IL loading and high temperature (*e.g.* 90–160 °C) to be effective.[14–18]

High boiling point solvents such as ethylene glycol (EG), ethylene carbonate (EC) and/or poly(ethylene glycol) (PEG) have been widely used as versatile chemicals in energy, plastic, automobile, surfactant, and electrolyte additive production.[19,20] These solvents have been shown to have potential applications in liquefaction of chitin, cellulose and biomass under acidic conditions,[21–26] in which EG or EG/EC is thought to participate in lignin removal and biomass defibrillation.[26] In these approaches, however, the solubilization of lignin was generally conducted at high temperatures (*e.g.* 90–200 °C), under acidic conditions, and with relatively high solvent/substrate ratios that are typically >10 : 1.[22] Moreover, a fundamental understanding of the interactions between lignin and the hydroxyl groups in these solvents is still absent and must be established in order to generate a robust lignin solubilization and depolymerization technology. Here we report an in-

[a]*Deconstruction Division, Joint BioEnergy Institute, Emeryville, CA, USA*
[b]*Biological and Engineering Sciences Center, Sandia National Laboratories, Livermore, CA, USA. E-mail: seesing@sandia.gov*
[c]*Environmental Molecular Sciences Laboratory, Pacific Northwest National Laboratory, Richland, WA, USA*
[d]*Biological Sciences Division, Pacific Northwest National Laboratory, Richland, WA, USA*
[e]*Biological Systems and Engineering Division, Lawrence Berkeley National Laboratory, Berkeley, CA, USA*

†Electronic supplementary information (ESI) available. See DOI: 10.1039/c6gc02258h

expensive, relatively non-toxic solvent, EG, that can quickly solubilize a large amount of lignin at room temperature. The solubilized lignin can be easily and quantitatively recovered by using simple anti-solvents such as ethanol, propanol and butanol. To explore the potential applications of this highly concentrated lignin solution, we used a low temperature approach to depolymerize the solubilized lignin using hydrogen peroxide. The mechanism of lignin solubilization and depolymerization in EG were elucidated using combined experimental and computational approaches.

Experimental section

Materials

Alkali lignin (typical molecular weight is 60 000 Da), ethylene glycol (anhydrous, 99.8%), glycerin (99.5%), ethylene carbonate (98%), propylene carbonate (99%), PEG200, PEG400, ethanol (anhydrous), 1-propanol (99.5%), 2-propanol (99.5%), 1-butanol (99.5%) and dimethyl sulfoxide (99.8%) were purchased from Sigma-Aldrich (St. Louis, MO) and used as received. 1-Ethyl-3-methylimidazolium acetate, abbreviated hereafter as $[C_2C_1Im][OAc]$, was purchased from BASF (Basionics™ BC-01, BASF, Florham Park, NJ). DMSO-d_6 was purchased from Cambridge Isotope Laboratories in Andover MA. Dilignol was synthesized following previously reported synthetic methodology.[27,28]

Solubilization, regeneration and depolymerization of lignin

Solubilization of lignin. In a typical process, 20 mL anhydrous ethylene glycol was placed into a 50 mL plastic tube. Alkali lignin was added in a stepwise fashion into the tube and simply mixed by vortexing until solubilized. Solubility of lignin in EG was confirmed by using a VWR Vista Vision Stereo Microscope with 20–40× magnification. The autofluorescence images of lignin during the solubilization and regeneration processes were collected with a Zeiss LSM 710 Confocal laser scanning fluorescence microscope (10× magnification, a 538 nm in tune laser).

Regeneration of lignin. A certain amount of ethanol was added into a 5 g alkali lignin solution and the system was simply mixed by vortexing. The regenerated lignin stream was separated by centrifugation (10 000 rpm, 10 min) and washed with ethanol (5 × 10 g). Thereafter, the collected alkali lignin was dried at 40 °C overnight under vacuum.

Depolymerization of lignin. 0.5 g alkali lignin solution (31 wt% in EG) and 3.5 g hydrogen peroxide (30 wt% in H_2O) were placed into a 15 mL glass pressure tube. The sealed tube was placed into an oil bath at 80 °C for 4 h. After the desired time, the tube was taken out from the oil bath and cooled to room temperature. Then, 5 mL ethyl acetate was added into the system to extract the lignin fractions. The ethyl acetate phase was analyzed by using SEC and GC-MS.

Lignin characterization

Nuclear magnetic resonance (NMR) spectroscopy. Data were acquired on a 600 MHz Varian Direct Drive (VNMRS) spectrometer using VNMRJ 4.0. The spectrometer system was outfitted with a Varian triple resonance salt-tolerant cold probe with a cold carbon preamplifier. All spectra were recorded with a temperature controlled at 25 °C. Samples were dissolved in DMSO-d_6.

Proton spectra were acquired as the first increment of a 2-D NOESY spectrum using the Varian tnnoesy.c pulse sequence, using a nonselective 90° excitation pulse, 50 ms mixing time, acquisition time of 2 s, a recycle delay of 1 s, spectral width of 12 ppm, and 16 transients per spectrum. Carbon spectra were acquired using s2pul.c with a nonselective 45° excitation pulse, acquisition time of 1 s, a recycle delay of 3 s, spectral width of 251 ppm, and 256 transients per spectrum.

To analyze the effect of EG concentration on ^{1}H chemical shifts of dilignol, 0.1 g (0.312 mmol) dilignol was dissolved in 600 μL of DMSO-d_6 at room temperature and was transferred to a NMR tube. Thereafter ^{1}H NMR spectra were recorded and referred to as 0 : 1 EG : dilignol. The samples of different incremental EG : dilignol molar ratios were prepared by sequentially adding molar equivalents of EG to the mixture.

Size exclusion chromatography (SEC). SEC was performed on the lignin in a liquid stream to understand the changes in lignin molecular weight distribution during the solubilization and depolymerization processes. An Agilent 1200 series binary LC system (G1312B) equipped with a DA (G1315D) detector was used. Separation was achieved with a Mixed-D column (5 mm particle size, 300 mm × 7.5 mm i.d., linear molecular weight range of 200 to 400 000 u, Polymer Laboratories, Amherst, MA) at 80 °C using a mobile phase of NMP at a flow rate of 0.5 mL min^{-1}. Absorbance of the materials eluting from the column was detected at 300 nm (UV-A).

Gas chromatography-mass spectrometry (GC-MS). Identification of chemical compounds in depolymerization products was carried out using an Agilent 6890N gas chromatograph equipped with an Agilent 5973N mass spectrometer. The capillary column used was an Agilent DB-5MS (30 m × 0.25 mm × 0.25 μm). The injection temperature was 250 °C and the oven temperature was programmed to hold at 50 °C for 1 min, ramp to 300 °C at 10 °C min^{-1} and then hold for additional 1 min.

Results and discussion

Lignin solubilization

Alkali lignin (Sigma-Aldrich, batch No. 1001044421) was used as a model lignin for solubilization experiments. As reported in Table 1, approximately 31 wt% lignin can be solubilized at room temperature (~20–23 °C) using EG as the solvent (Table 1, entry 1), whereas the IL $[C_2C_1Im][OAc]$ did not (entry 2). On heating to 80 °C, only 18 wt% of lignin can be dissolved in $[C_2C_1Im][OAc]$ (entry 3). We also investigated lignin solubilization using low molecular weight polyethylene glycol (PEG). For PEG with molecular weights of 200 or 400 (PEG 200 and PEG 400; entries 4 and 5) as the solvents, much lower lignin solubilities were observed compared to those observed in EG

Table 1 Solubilization of alkali lignin in different solvents[a]

Entry	Solvents	Temperature (°C)	Solubility[b] (wt%)
1	EG	20	31
2	$[C_2C_1Im][OAc]$	20	1
3	$[C_2C_1Im][OAc]$	80	18
4	PEG200	20	2
5	PEG400	20	1
6	Glycerol	20	25
7	EC	50	Insoluble
8	PC	20	Insoluble
9	Ethanol	20	Insoluble
10	1-Propanol	20	Insoluble
11	2-Propanol	20	Insoluble
12	1-Butanol	20	Insoluble
13[c]	EG	20	>35
14[d]	EG	20	35

[a] Conditions: solvent 5 g, room temperature. [b] Solubility was determined by using a VWR Vista Vision Stereo Microscope with 20–40× magnification. [c] Enzymatic mild acidolysis lignin EMAL (from switchgrass). [d] Lignin fraction generated from cholinium lysinate ([Ch][Lys]) pretreatment of switchgrass.[7]

indicating that there is no significant effect of the molecular weight of PEG on the solubility of lignin. We hypothesize that this low solubility can be attributed to the relatively high viscosity of the PEGs used,[29] combined with the low density of hydroxyl groups and the weak hydrogen bond network compared to EG. Using solvents with multiple hydrogen donor sites like glycerol, approximately 25 wt% of alkali lignin solubilization can be achieved at room temperature (entry 6). The rapid and higher amount of alkali lignin dissolution in EG might be related to its lower viscosity (0.0162 N s m^{-2}, 25 °C) compared to glycerol (0.95 N s m^{-2}, 25 °C). Negligible solubility was detected in the cases of ethylene carbonate (EC), propylene carbonate (PC), ethanol, 1-propanol, 2-propanol, and 1-butanol at room temperature (entries 7–12). In addition, EG also exhibited high solubilization of enzymatic mild acidolysis lignin (EMAL) and the lignin fraction generated from cholinium lysinate ([Ch][Lys]) pretreatment of switchgrass (entries 13 and 14) at room temperature. The above results indicate that EG is a very effective solvent for lignin at room temperature.

Fig. 1 depicts the processes of rapid dissolution and regeneration of lignin at room temperature. We found that 31 wt% lignin can be completely dissolved in EG (Fig. 1A) by simple mixing and the resulting solution is dark and highly viscous (Fig. 1B). The dissolved lignin can be precipitated immediately by adding ethanol (Fig. 1C) and easily recovered by centrifugation. Besides ethanol, solvents such as 1-propanol, 2-propanol and 1-butanol can also be used as an anti-solvent for the

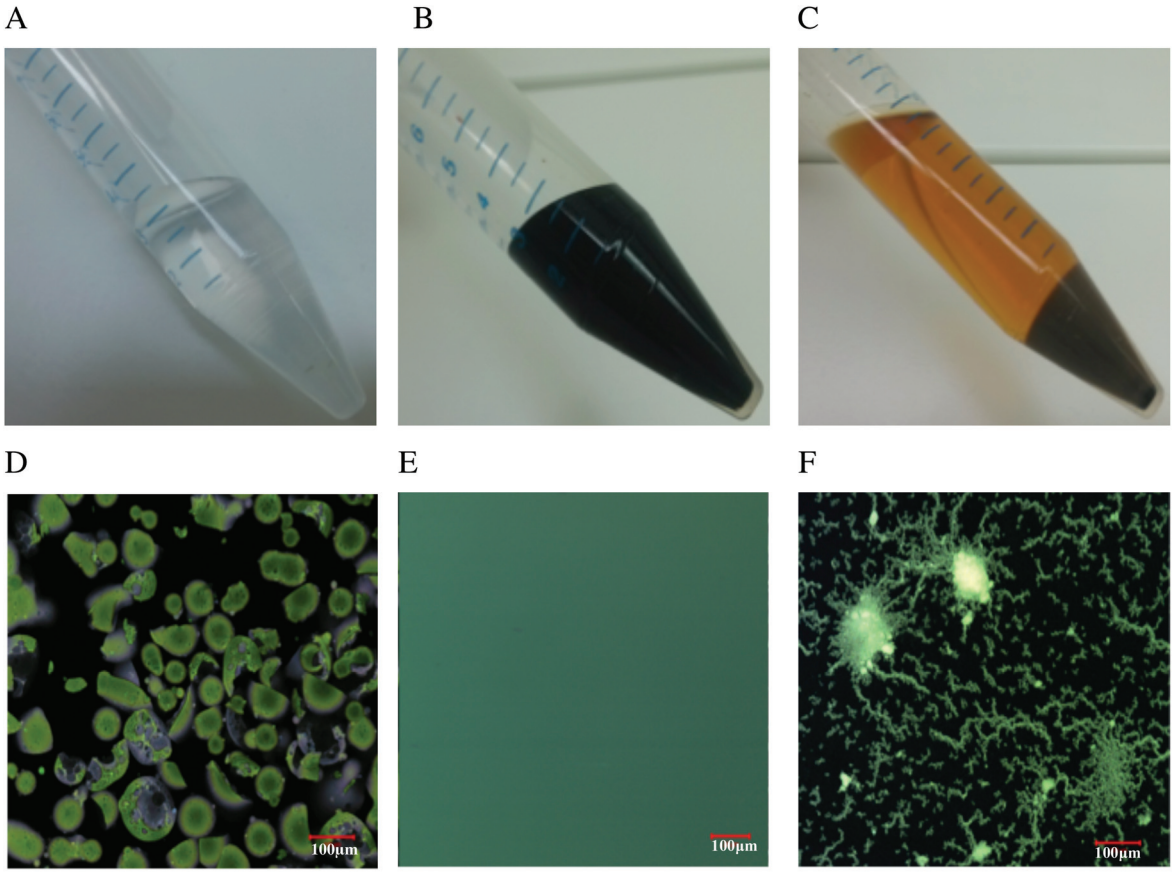

Fig. 1 Rapid solubilization and regeneration of alkali lignin at room temperature: (A) EG; (B) EG/lignin and (C) EG/lignin/ethanol. Fluorescence microscopy results (10×): (D) native alkali lignin (20×); (E) lignin/EG solution (10×) and F) regenerated lignin (10×).

lignin–EG system. This simple isolation of dissolved lignin will enable EG recovery and lignin purification. Confocal microscopy (10× magnification) was used to explore the morphological changes of lignin during the solubilization and regeneration processes, and the results are shown in Fig. 1. The fluorescence resulting from native lignin particles can be seen and approximately spherical porous particles were observed at 10× magnification under these conditions (Fig. 1D). After solubilization in EG, a homogenous system with an enhanced fluorescence intensity (Fig. 1E) and no visible particles was observed. After the use of ethanol as the anti-solvent, the fluorescence related to the precipitated lignin microfibrils (>20 μm) was observed (Fig. 1F). The lignin recovery was observed to be directly proportional to the weight ratio of ethanol to EG in the system, with lignin recoveries of 3.5, 80.5 and 97.3 wt% obtained at weight ratios of 0.5, 2 and 4, respectively (Fig. S1, ESI†). The increase in the recovery of lignin with an increasing amount of ethanol is hypothesized to occur due to the ethanol molecules shielding the EG molecules, and thus direct interactions between lignin and EG molecules are weakened. This process is thought to be similar with cellulose precipitation from ionic liquid solutions by the addition of anti-solvents.[30]

Understanding the mechanism of lignin solubilisation in EG

Based on the above results, EG demonstrated extraordinary solubility of lignin compared to the other organic solvents tested in this work. In-depth investigation of the interactions between EG and lignin was conducted to understand its high solubility. Considering the complex and heterogeneous nature of lignin, it is very difficult to conduct a mechanistic study directly by using computational simulation. For this reason, lignin model compounds are commonly used for mechanistic research instead of macromolecular lignin.[7,31,32] Since dilignol, such as a β-O-4 dimer (see Fig. 2G for structure), represents 50–80% inter-unit linkages depending on the origin,[8] this model dimer was used to understand the relationship between the hydrogen bond interactions and the solvation properties of EG at the molecular level.

Several different molecular conformations and geometries are possible for the dilignol–EG interaction owing to the structural flexibility of EG and dilignol. To obtain the most stable structures of the dilignol–EG complex, many starting complexes were considered based on the intermolecular hydrogen bond between the EG molecules and the hydroxyl groups of dilignol. Fifteen initial geometries were considered in each case and optimized at the M06-2X/6-31+G (d, p) level of theory. Harmonic frequencies at the same level of theory were calculated to ensure that the clusters were true minima. The most stable structures of dilignol–EG were classified according to the interaction of EG with (1) the α-C hydroxyl group (α-OH), (2) the γ-C hydroxyl group (γ-OH) and (3) the phenolic hydroxyl group (ring-OH). These complexes were optimized at a higher M06-2X/6-311+G (2d, 2p) level of theory using the G09 suite of programs.[33]

IEs were calculated using a supermolecular approach and corrected for basis set superposition error (BSSE) using the counterpoise (CP) procedure suggested by Boys and Bernardi,[33] which is provided in the equation below:

$$\mathrm{IE} = -\left(E_{\mathrm{complex}} - \left(\sum_{i=1}^{m} E_{\mathrm{Lignol}} + \sum_{j=1}^{n} E_{\mathrm{EG}_j}\right)\right) \quad (1)$$

where E_{Complex} refers to the total energies of dilignol with EGs, and E_{Lignol} and E_{EG_j} are the total energies of the dilignol and EG, respectively.

The geometries of the dilignol–EG complexes optimized at the M06-2X/6-311++G (2d, 2p) level of theory are presented in Fig. 2, along with their hydrogen bond distances. Both hydroxyl groups of the EG molecule participate in the hydrogen bond interactions with dilignol hydroxyl groups. Some of the vibrational frequencies of individual molecules undergo substantial shifts and the changes in the frequencies provide information about the characteristics of the interaction between the molecules. A red shift in the hydroxyl group stretching frequencies (ν_{OH}) has been used to characterize hydrogen bond formation. Therefore, vibrational frequencies for the isolated dilignol hydroxyl groups and their interaction with EG have been calculated at the same level. The calculated (scaled) frequencies of individual ring-OH and γ-OH are 3710 and 3741 cm^{-1}, respectively. However, in the dilignol–EG complexes, the calculated ν_{OH} stretches occur at 3483 and 3581 cm^{-1}, respectively. The red shifts of these modes from those of isolated hydroxyl groups are 227 and 160 cm^{-1}, respectively, indicating strong hydrogen bond formation upon dilignol solvation by using EG. The complex with EG interacting with the dilignol γ-OH (Fig. 2B *vs.* Fig. 2A and B) is the most stable one, with a cyclic intermolecular hydrogen bond network involving the hydroxyl group and the ether bond oxygen atom. There is a steady increase in the interaction energy (IE) present in the complexes of dilignol with two and three EG molecules (Fig. 2D and E). In order obtain a more relevant model for experimental lignin dissolution in EG, a complex containing ten EG molecules solvating one dilignol molecule was investigated, in which the weight ratio of dilignol to EG is around 34 : 66 (Fig. 2F). The optimization was carried out using B3LYP/6-31G* in Terachem and single point calculations at the M06-2X/6-311+G (2d, 2p) level of theory used to obtain the IE of the complex. Fig. 2F shows that the ten EG molecules completely solvated the dilignol by forming an intermolecular hydrogen bond network. The calculated IEs indicate cooperativity in the hydrogen bond in the solvation of lignin by EG. Also, it is hypothesized that in these complexes, both electrostatic and polarization interactions are the predominant determinants of the structural properties of dissolution, and that the dynamic properties are primarily influenced by the viscosity of the polar EG solvent.

It has been proposed that the interaction of IL (*i.e.* 1-allyl-3-methylimidazolium chloride) with lignin is stronger than that of lignin with lignin; thus lignin can be dissolved in ILs.[34] To further verify the interactions between a non-IL solvent (*i.e.* EG) and lignin, the effect of EG on the proton chemical shifts of lignin was investigated using NMR spectroscopy. The chemi-

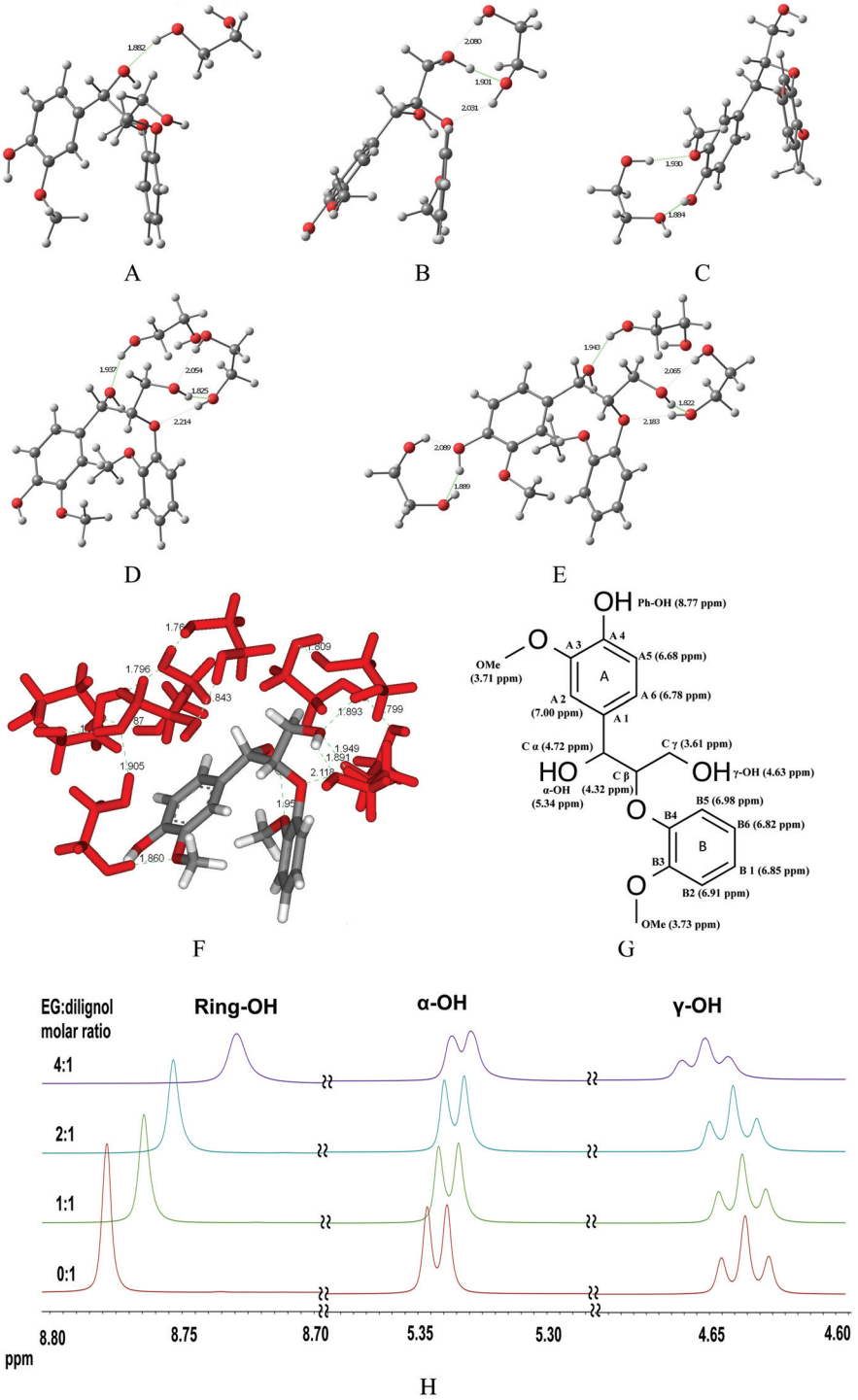

Fig. 2 Optimized geometries of dilignol–EG complexes (A–F), ^{1}H NMR chemical shift assignment of dilignol in DMSO-d_6 (G), and the effect of EG concentration on the ^{1}H NMR chemical shifts of ring-OH, α-OH, and γ-OH of dilignol (H). Only the ring-OH and the hydroxyl protons are depicted. Interaction energy (IE) is reported in kcal mol^{-1}. (A) Dilignol–EG_1 (α-OH), IE = 8.39; (B) Dilignol–EG_1 (γ-OH), IE = 12.2; (C) Dilignol–EG_1 (ring-OH), IE = 11.2; (D) Dilignol–EG_2, IE = 22.9; (E) Dilignol–EG_3, IE = 33.8; (F) Dilignol–EG_{10} (EG shown in red), IE = 133.4.

cal shift assignments of the dilignol (Fig. 2G) were made using 2-D ^{1}H–^{1}H COSY, ^{1}H–^{13}C HSQC and HMBC experiments. Putative sites on the dilignol molecule that participate in the interaction with EG were identified from the chemical shift perturbations during the titration of EG into the dilignol solution. The effect of EG concentration on the shielding or deshielding of hydroxyl and phenolic protons in dilignol is shown in Fig. 2H. The proton of the ring-OH, which is the most acidic proton in dilignol, demonstrates the greatest upfield shift with the increasing EG concentration compared

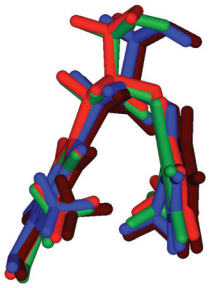

	RMSD (Å)
Dilignol	-
Dilignol-EG_1	1.24
Dilignol-EG_3	1.40
Dilignol-EG_{10}	5.70

Fig. 3 Superimposed structures of the bare dilignol (blue) and isolated dilignol–EG_1 (green), dilignol–EG_3 (brown), and dilignol–EG_{10} (red) complexes and the overall influence of the geometrical variations (root mean square deviations, RMSD).

to the other dilignol protons. This is contrary to the expected downfield shift due to the formation of a hydrogen bond. However, in the absence of EG the dilignol molecules are intermolecularly hydrogen bonded. In the presence of EG, the strong intermolecular hydrogen bonds between the dilignol molecules are replaced by the relatively weak hydrogen bonds between the H-atom of ring-OH and the O-atom of an EG molecule, which could result in the observed strong upfield shift of the ring-OH proton. A downfield shift was observed for the γ-OH proton, suggesting a relatively strong hydrogen bond between the γ-OH proton and EG.

To compare the influence of the EG interactions with dilignol, the bare dilignol and the dilignol from the complexes were superimposed (Fig. 3) to gain insights into the overall influence of the geometrical variations (root mean square deviations, RMSD). We carried out calculations on a water molecule interacting with dilignol (Fig. S2, ESI†) and the structural change was analyzed. The dilignol structure is not much influenced by water (0.3Å) interactions, but the dilignol–EG_1 (molar ratio of dilignol to EG is 1 : 1) complex induced noticeable variation in dilignol conformations. Likewise, dilignol from the dilignol–EG_3 complex also underwent more conformational changes from the bare dilignol than the dilignol in water. The superimposed model of the dilignol–EG_{10} also indicates that there is significant variation in the conformation from the bare dilignol to this complex. This observation suggests that the dilignol conformation is affected by the hydrogen bond interactions of EG molecules, and that overall EG solvation changes the viscoelastic properties of lignin at room temperature, which could be the possible reason for the prominent solubility.

Depolymerization of solubilized lignin

After exploring the possible lignin dissolution mechanism in EG, we further attempted to test the mild oxidative depolymerization of this highly concentrated lignin solution at 80 °C. H_2O_2 (30 wt% in H_2O) was used as the oxidant for the depolymerization of lignin under mild reaction conditions. Fig. 4A depicts the elugram of the SEC profiles of alkali lignin and its depolymerization reaction mixture. In this work, we are using the established methods to measure the lignin molecular weight to compare the relative changes in the molecular weight of lignin during the depolymerization process.[35–37] As shown in the figure the main lignin backbone peak slightly shifted toward the low molecular weight region. In addition, two new peaks centered at around 18.5 to 20.5 min appeared in the elugram of the depolymerization reaction mixture, which have comparable retention times with dilignol and monolignol (vanillyl alcohol), respectively. This indicated that the depolymerization of lignin could occur at low temperatures.

The oxidative action of the H_2O_2 derived radicals is thought to contribute to lignin depolymerization by fragmenting the lignin macrostructure into a number of low molecular weight compounds.[38] However, this corresponding process is too complex to be understood without considerable effort. Thus, dilignol was used to compare the depolymerization products from lignin. In our EG/H_2O_2 system, it was also hypothesized that lignin depolymerization follows a peroxidative cleavage mechanism, which is similar to the previous studies on the degradation of lignin in the presence of H_2O_2.[39,40] The depolymerization products were identified by GC-MS (Fig. 4B). The vanillic acid and guaiacol are the primary products identified by GC-MS from the oxidative reactions of dilignol and alkali lignin. A relatively high amount of vanillic acid was found in the presence of EG.

Mechanistic understanding of H_2O_2 enabled depolymerization of lignin solubilized in EG

The observation of vanillic acid and guaiacol among the reaction products prompted us to probe the molecular level details of the depolymerization reactions of EG-solvated lignin in the presence of H_2O_2. The reactions and products are akin to lignin degradation by fungal and bacterial systems.[41–44] In fungal ligninases (peroxidative cleavage), a single electron transfer (SET) charge transport process is involved in the production of cation radicals that induce degradation by cleaving lignin linkages.[45] Another study shows that bacterial strains convert coniferyl alcohol to the intermediates coniferylaldehyde, ferulic acid, vanillic acid and finally to protocatechuic acid.[46] Multi-step lignin degradation pathways have been demonstrated in biotic environments and these require multiple enzymes with a variety of cofactors.[47] To determine the factors involved in the bio-mimicking reactions in an abiotic system, the charge transfer analyses and bond dissociation energy profiles involved in the initiation of the dilignol–EG_1–H_2O_2 complexes were studied in detail. The natural bond orbital (NBO) approach is a convenient means to understand the donor–acceptor interaction and to decompose the various important interactions present in the hydrogen bond complexes, including the charge transfer (CT) component which is associated with partial electron transfer.[48,49] The NBO second-order interaction energies are calculated and listed in Table 2 for dilignol (γ-OH)–EG_1 and dilignol (γ-OH)–EG_1–H_2O_2. Atom numbering of these complexes and fragments used for NBO analysis are shown in Fig. S3, ESI.† It can be seen that every

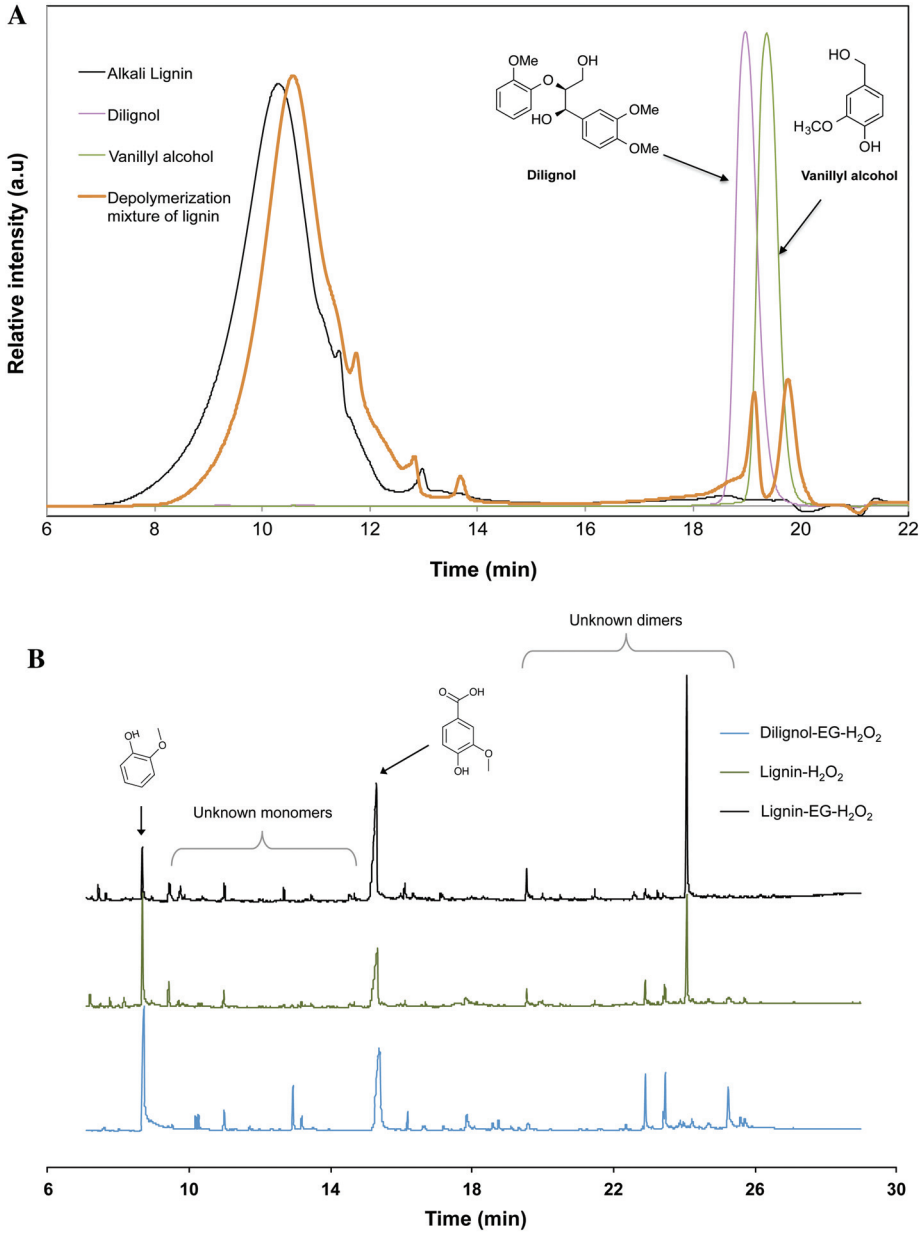

Fig. 4 Analysis of depolymerization of dissolved lignin (A, SEC, and B, GC-MS).

single hydrogen bond has a second-order interaction energy contributing to the stability of the complexes.

The interaction, n(O) → σ*(O–H), describes the partial CT or donor–acceptor interaction between the non-bonding orbital (lone pair) of the O atom and the anti-bonding orbital of the O–H. As expected, for each interaction, there is a considerable amount of partial electron transfer from n(O) to σ* (O–H). For the dilignol–EG_1, the sum of partial CT interaction is 17.9 kcal mol^{-1}. The respective CT interaction for dilignol (γ-OH)–EG_1–H_2O_2 is 44.23 kcal mol^{-1}. It is interesting to note that CT interaction energy of dilignol (fragment 1) to EG (fragment 2) is higher for dilignol (γ-OH)–EG_1–H_2O_2 than for dilignol–EG_1. The CT interaction energy in dilignol (γ-OH)–EG_1–H_2O_2 from EG (fragment 2) to H_2O_2 is 19.18 kcal mol^{-1} and in the H_2O_2 (fragment 3) to dilignol (fragment 1) is 8.33 kcal mol^{-1}. These variations clearly indicate that each CT interaction is different and that CT interactions in dilignol–EG_1 contribute to the stability of the solvated complexes. On the other hand, it is evident from the significant CT interactions in dilignol (γ-OH)–EG_1–H_2O_2 complexes that the presence of H_2O_2 increases the CT from dilignol to EG to H_2O_2 to dilignol and that this could be one of the main factors contributing to lignin dissociation in the presence of H_2O_2. The weakening of lignin linkages upon H_2O_2 interactions destabilizes the C–C and C–O bonds, initiating the bond cleavage reaction from ether linkages to form guaiacol and vanillic acid

Table 2 Donor orbitals (ϕ_i), acceptor orbitals (ϕ_j), and the corresponding second-order interaction energies of dilignol–EG_1 (γ-OH) and dilignol–EG_1 (γ-OH)–H_2O_2 complexes

System	Fragment	$\phi_i \rightarrow \phi_j$	$\Delta E_{ij}^{(2)}$ kcal mol^{-1}
Dilignol–EG_1 (γ-OH)	Fragment 1 to 2	n(O)15 → σ*(O10–H52)	3.47
		n(O)26 → σ*(O51–H53)	4.56
	Fragment 2 to 1	n(O)50 → σ*(O26–H27)	9.87
Dilignol–EG_1 (γ-OH)–H_2O_2	Fragment 1 to 2	n(O)26 → σ*(O51–H53)	7.74
		n(O)38 → σ*(O50–H52)	7.52
	Fragment 2 to 3	n(O)50 → σ*(O54–H57)	19.2
	Fragment 3 to 1	n(O)55 → σ*(O26–H27)	8.33

by further oxidative cleavage at the α-C position. These biomimicking chemical catalytic routes are powerful compared to biotic systems studied to date and hydroxylation, decarboxylation or demethylation reactions of various sites could serve to generate new chemical routes for future market demands.

Conclusions

Rapid room temperature solubilization of lignin at >30 wt% solid loading was achieved within 10 min using ethylene glycol (EG). The results indicated that both hydroxyl groups of the EG molecule participate in hydrogen bond interactions with lignin. ^{1}H NMR spectra demonstrated that the proton of the phenolic-hydroxyl group, which is the most acidic proton in dilignol, experiences the greatest interactions with the EG molecule compared to the other dilignol protons. The computational studies revealed possible hydrogen bond interacting complexes between EG and dilignol and ensured the presence of cyclic intermolecular hydrogen bond network involving the hydroxyl group and the ether bond oxygen atom. The addition of anti-solvents such as ethanol, promotes a fast and high recovery (~97 wt%) of dissolved lignin allowing easy solvent recycling. Monomeric lignins such as vanillic acid and guaiacol were produced from the depolymerization of solubilized lignin in the presence of H_2O_2 under mild conditions. The present work provides an effective way to generate highly concentrated lignin solution, which can be further utilized for chemical conversion and different materials applications. More efforts are still warranted to improve the solubility of the initial lignin in real lignocellulosic biomass using EG based technology and explore new applications of the lignin–EG system in biological and material fields.

Acknowledgements

This work conducted by the Joint BioEnergy Institute was supported by the Office of Science, Office of Biological and Environmental Research of the U.S. Department of Energy under contract no. DE-AC02-05CH11231. A portion of the research was performed using EMSL, a DOE Office of Science User Facility sponsored by the Office of Biological and Environmental Research located in the Pacific Northwest National Laboratory. The United States Government retains and the publisher, by accepting the article for publication, acknowledges that the United States Government retains a non-exclusive, paid-up, irrevocable, worldwide license to publish or reproduce the published form of this manuscript, or allow others to do so, for United States Government purposes. The back cover image was designed and produced by Mr. Rui Sun.

References

1 C. Z. Li, X. C. Zhao, A. Q. Wang, G. W. Huber and T. Zhang, *Chem. Rev.*, 2015, **115**, 11559–11624.
2 A. J. Ragauskas, G. T. Beckham, M. J. Biddy, R. Chandra, F. Chen, M. F. Davis, B. H. Davison, R. A. Dixon, P. Gilna, M. Keller, P. Langan, A. K. Naskar, J. N. Saddler, T. J. Tschaplinski, G. A. Tuskan and C. E. Wyman, *Science*, 2014, **344**, 709–720.
3 J. Zakzeski, P. C. A. Bruijnincx, A. L. Jongerius and B. M. Weckhuysen, *Chem. Rev.*, 2010, **110**, 3552–3599.
4 B. M. Upton and A. M. Kasko, *Chem. Rev.*, 2016, **116**, 2275–2306.
5 W. J. Liu, H. Jiang and H. Q. Yu, *Chem. Rev.*, 2015, **115**, 12251–12285.
6 T. J. Morgan and R. Kandiyoti, *Chem. Rev.*, 2014, **114**, 1547–1607.
7 M. P. Pandey and C. S. Kim, *Chem. Eng. Technol.*, 2011, **34**, 29–41.
8 R. Rinaldi, R. Jastrzebski, M. T. Clough, J. Ralph, M. Kennema, P. C. A. Bruijnincx and B. M. Weckhuysen, *Angew. Chem., Int. Ed.*, 2016, **55**, 8164–8215.
9 Z. Strassberger, S. Tanase and G. Rothenberg, *RSC Adv.*, 2014, **4**, 25310–25318.
10 G. T. Beckham, C. W. Johnson, E. M. Karp, D. Salvachúa and D. R. Vardon, *Curr. Opin. Biotechnol.*, 2016, **42**, 40–53.
11 Z. Strassberger, P. Prinsen, F. van der Klis, D. S. Van Es, S. Tanase and G. Rothenberg, *Green Chem.*, 2015, **17**, 325–334.
12 L. da Costa Sousa, M. Foston, V. Bokade, A. Azarpira, F. Lu, A. J. Ragauskas, J. Ralph, B. Dale and V. Balan, *Green Chem.*, 2016, **18**, 4205–4215.
13 E. C. Achinivu, R. M. Howard, G. Q. Li, H. Gracz and W. A. Henderson, *Green Chem.*, 2014, **16**, 1114–1119.

14 L. Mu, Y. Shi, L. Chen, T. Ji, R. Yuan, H. Wang and J. Zhu, *Chem. Commun.*, 2015, **51**, 13554–13557.
15 N. Sun, R. Parthasarathi, A. M. Socha, J. Shi, S. Zhang, V. Stavila, K. L. Sale, B. A. Simmons and S. Singh, *Green Chem.*, 2014, **16**, 2546–2557.
16 W. E. S. Hart, J. B. Harper and L. Aldous, *Green Chem.*, 2015, **17**, 214–218.
17 J. Sun, N. V. S. N. M. Konda, J. Shi, R. Parthasarathi, T. Dutta, F. Xu, C. D. Scown, B. A. Simmons and S. Singh, *Energy Environ. Sci.*, 2016, **9**, 2822–2834.
18 T. Dutta, J. Shi, J. Sun, X. Zhang, G. Cheng, B. A. Simmons and S. Singh, *Ionic Liquids in the Biorefinery Concept: Challenges and Perspectives*, Royal Society of Chemistry, 2016, pp. 65–94, DOI: 10.1039/9781782622598-00065.
19 H. R. Yue, Y. J. Zhao, X. B. Ma and J. L. Gong, *Chem. Soc. Rev.*, 2012, **41**, 4218–4244.
20 S. Komaba, T. Ishikawa, N. Yabuuchi, W. Murata, A. Ito and Y. Ohsawa, *ACS Appl. Mater. Interfaces*, 2011, **3**, 4165–4168.
21 T. Zhang, Y. Zhou, D. Liu and L. Petrus, *Bioresour. Technol.*, 2007, **98**, 1454–1459.
22 E. Jasiukaitytė, M. Kunaver and M. Strlič, *Cellulose*, 2009, **16**, 393–405.
23 A. Krzan and E. Zagar, *Bioresour. Technol.*, 2009, **100**, 3143–3146.
24 D. H. Lee, E. Y. Cho, C. J. Kim and S. B. Kim, *Biotechnol. Bioprocess Eng.*, 2010, **15**, 1094–1101.
25 Y. Pierson, X. Chen, F. D. Bobbink, J. G. Zhang and N. Yan, *ACS Sustainable Chem. Eng.*, 2014, **2**, 2081–2089.
26 Z. Zhang, I. M. O'Hara, D. W. Rackemann and W. O. S. Doherty, *Green Chem.*, 2013, **15**, 255–264.
27 J. Buendia, J. Mottweiler and C. Bolm, *Chem. – Eur. J.*, 2011, **17**, 13877–13882.
28 A. Rahimi, A. Azarpira, H. Kim, J. Ralph and S. S. Stahl, *J. Am. Chem. Soc.*, 2013, **135**, 6415–6418.
29 N. V. Zivkovic, S. S. Serbanovic, M. L. Kijevcanin and E. M. Zivkovic, *J. Chem. Eng. Data*, 2013, **58**, 3332–3341.
30 P. Maki-Arvela, I. Anugwom, P. Virtanen, R. Sjoholm and J. P. Mikkola, *Ind. Crops Prod.*, 2010, **32**, 175–201.
31 J. B. Binder, M. J. Gray, J. F. White, Z. C. Zhang and J. E. Holladay, *Biomass Bioenergy*, 2009, **33**, 1122–1130.
32 T. He, Y. M. Zhang, Y. A. Zhu, W. Wen, Y. Pan, J. L. Wu and J. H. Wu, *Energy Fuels*, 2016, **30**, 2204–2208.
33 S. F. Boys and F. Bernardi, *Mol. Phys.*, 2002, **100**, 65–73.
34 W. Y. Ji, Z. D. Ding, J. H. Liu, Q. X. Song, X. L. Xia, H. Y. Gao, H. J. Wang and W. X. Gu, *Energy Fuels*, 2012, **26**, 6393–6403.
35 A. George, K. Tran, T. J. Morgan, P. I. Benke, C. Berrueco, E. Lorente, B. C. Wu, J. D. Keasling, B. A. Simmons and B. M. Holmes, *Green Chem.*, 2011, **13**, 3375–3385.
36 N. Sathitsuksanoh, K. M. Holtman, D. J. Yelle, T. Morgan, V. Stavila, J. Pelton, H. Blanch, B. A. Simmons and A. George, *Green Chem.*, 2014, **16**, 1236–1247.
37 J. Shi, S. Pattathil, R. Parthasarathi, N. A. Anderson, J. I. Kim, S. Venketachalam, M. G. Hahn, C. Chapple, B. A. Simmons and S. Singh, *Green Chem.*, 2016, **18**, 4884–4895.
38 M. J. Selig, T. B. Vinzant, M. E. Himmel and S. R. Decker, *Appl. Biochem. Biotechnol.*, 2009, **155**, 397–406.
39 T. K. Kirk and R. L. Farrell, *Annu. Rev. Microbiol.*, 1987, **41**, 465–501.
40 H. B. Zhu, Y. M. Chen, T. F. Qin, L. Wang, Y. Tang, Y. Z. Sun and P. Y. Wan, *RSC Adv.*, 2014, **4**, 6232–6238.
41 K.-E. L. Eriksson, R. Blanchette and P. Ander, *Microbial and enzymatic degradation of wood and wood components*, Springer Science & Business Media, 2012.
42 T. Higuchi, in *New Trends in Research and Utilization of Solar Energy through Biological Systems*, ed. H. Mislin and R. Bachofen, Birkhäuser Basel, Basel, 1982, pp. 87–94, DOI: 10.1007/978-3-0348-6305-6_19.
43 M. E. Brown, M. C. Walker, T. G. Nakashige, A. T. Iavarone and M. C. Y. Chang, *J. Am. Chem. Soc.*, 2011, **133**, 18006–18009.
44 T. D. H. Bugg, M. Ahmad, E. M. Hardiman and R. Rahmanpour, *Nat. Prod. Rep.*, 2011, **28**, 1883–1896.
45 D. W. Cho, R. Parthasarathi, A. S. Pimentel, G. D. Maestas, H. J. Park, U. C. Yoon, D. Dunaway-Mariano, S. Gnanakaran, P. Langan and P. S. Mariano, *J. Org. Chem.*, 2010, **75**, 6549–6562.
46 L. Eggeling and H. Sahm, *Arch. Microbiol.*, 1980, **126**, 141–148.
47 T. D. H. Bugg, M. Ahmad, E. M. Hardiman and R. Singh, *Curr. Opin. Biotechnol.*, 2011, **22**, 394–400.
48 A. E. Reed, L. A. Curtiss and F. Weinhold, *Chem. Rev.*, 1988, **88**, 899–926.
49 R. Parthasarathi, V. Subramanian and N. Sathyamurthy, *Synth. React. Inorg., Met.-Org., Nano-Met. Chem.*, 2008, **38**, 18–26.

